

# COMISR: Compression-Informed Video Super-Resolution

Yinxiao Li, Pengchong Jin, Feng Yang, Ce Liu, Ming-Hsuan Yang, and Peyman Milanfar

Google Inc.

## Abstract

Most video super-resolution methods focus on restoring high-resolution video frames from low-resolution videos without taking into account compression. However, most videos on the web or mobile devices are compressed, and the compression can be severe when the bandwidth is limited. In this paper, we propose a new compression-informed video super-resolution model to restore high-resolution content without introducing artifacts caused by compression. The proposed model consists of three modules for video super-resolution: bi-directional recurrent warping, detail-preserving flow estimation, and Laplacian enhancement. All these three modules are used to deal with compression properties such as the location of the intra-frames in the input and smoothness in the output frames. For thorough performance evaluation, we conducted extensive experiments on standard datasets with a wide range of compression rates, covering many real video use cases. We showed that our method not only recovers high-resolution content on uncompressed frames from the widely-used benchmark datasets, but also achieves state-of-the-art performance in super-resolving compressed videos based on numerous quantitative metrics. We also evaluated the proposed method by simulating streaming from YouTube to demonstrate its effectiveness and robustness.

## 1. Introduction

Super-resolution is a fundamental research problem in computer vision with numerous applications. It aims to reconstruct detailed high-resolution (HR) image(s) from low-resolution (LR) input(s). When the input is one single image, the reconstruction process usually uses learned image priors to recover high-resolution details of the given image, which is called single image super-resolution (SISR) [55]. When numerous frames in a video are available, the reconstruction process uses both image priors and inter-frame information to generate temporally smooth high-resolution results, which is known as video super-resolution (VSR).

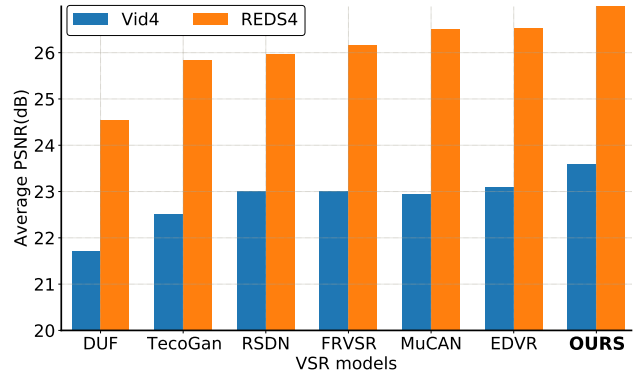


Figure 1. Video super-resolution results (4×, RGB-channels) on compressed Vid4 and REDS datasets. Here we show the results using the most widely adopted compression rate (CRF 23 [10]).

Although great progress has been made, existing SISR and VSR methods rarely take into account compression. In this paper, we say that previous work used *uncompressed* data to emphasize the high-quality, low-compression-ratio videos. As such, previous methods tend to generate significant artifacts when operated on heavily compressed input videos. However, most videos on the web or mobile devices are stored/streamed with different levels of compression to achieve a selected visual quality level. For example, a popular compression rate (Constant Rate Factor (CRF)) for H.264 encoding is 23 as a trade-off between quality and file size. We applied such setting to a few VSR evaluation datasets, and noticed that all the state-of-the-art VSR algorithms that we tested did not perform as well when videos are compressed, as shown in Figure 4 and Figure 5.

One possible solution is applying a denoising model [57, 34, 35] to remove compression artifacts, followed by one of the state-of-the-art VSR models. At first glance, this is appealing since a VSR model is fed with high-quality frames, similar to directly using the evaluation data, such as Vid4 [31]. However, our experiments in Section 4.3 indicate that such setting would not boost the final performance; it might even make it worse. With pre-processing, it is highly likely that the denoising model in the first step will change

the degradation kernel used implicitly in the VSR model training. So essentially, the VSR models are being applied to more challenging data.

Another possible solution is training the existing state-of-the-art VSR models on the compressed frames. This can bring additional compression information to the model training. However, our experiments described in Section 4.5 indicate that simply using compressed frame in training brings only modest improvement. In fact, without specific changes to the designs of network modules, such training data may even hurt the overall performance.

To alleviate the above-mentioned issues, we propose a compression-informed (i.e., compression-aware) super-resolution model that can perform well on real-world videos with different levels of compression. Specifically, we designed three modules to robustly restore the missing information caused by video compression. First, a bi-directional recurrent module is developed to reduce the accumulated warping error from the random locations of the *intra-frame* from compressed video frames [45]. Second, a detail-aware flow estimation module is added to enable recovery of HR flow from compressed LR frames. Finally, a Laplacian enhancement module adds high-frequency information to the warped HR frames washed out by video encoding. We refer to this overall model as *COMpression-Informed video Super-Resolution (COMISR)*.

With the proposed COMISR model, we demonstrated the effectiveness of the three modules with ablation studies. We conducted extensive experiments on several VSR benchmark datasets, including Vid4 [31] and REDS4 [40], with videos compressed with different CRF values. We showed that the COMISR model achieves significant performance gain on compressed video (e.g., CRF23), as shown in Figure 1; and meanwhile maintains competitive performance on uncompressed video. In addition, we showed evaluation results based on different combinations of a state-of-the-art VSR model and an off-the-shelf video denoiser. Finally, we demonstrated the robustness of the COMISR model on simulating streaming YouTube videos, which are compressed with proprietary encoders.

The contributions of this paper can be summarized as:

- We introduced a compression-informed model for super-resolving real-world compressed videos for practical applications.
- We incorporated three modules that are novel to VSR to effectively improve the critical components for video super-resolution on compressed frames.
- We conducted extensive experiments of state-of-the-art VSR models on compressed benchmark datasets. We also provided a new setting of evaluating the VSR models from YouTube transcoding output, which is a real-world application scenario beyond all existing evaluation methods.

## 2. Related Work

A plethora of super-resolution methods have been developed in the literature based on variational formulations [60] or deep neural networks [55, 61, 1]. In this section, we discuss recent deep models closely related to our work for super-resolution.

### 2.1. Single Image super-resolution

Dong *et al.* [8] propose the SRCNN model based on convolutional neural networks for single image super-resolution. Based on the residual learning framework [18], Kim *et al.* propose the VDSR [23] and DRCN [24] models for more effective image super-resolution. To speed up the network, Dong *et al.* [9] use a deconvolution layer at the end of the network to directly learn the mapping from low-resolution to high-resolution images. Similarly, Shi *et al.* introduce the ESPCN [46] model with an efficient sub-pixel convolution layer at the end of the network. In the LatticeNet method [37], a light-weighted model is developed by using a lattice block, which reduces half amount of the parameters while maintaining similar SR performance. To deal with large scaling factors, Lai *et al.* [26] develop the LapSRN model which progressively recovers the sub-band residuals of high-resolution images. Instead of relying on deeper models, the MemNet [47] introduce memory block to exploit long-term dependency for effective SR models. On the other hand, the SRDenseNet [49] and RDN [68] solve SISR with dense connections based on the DenseNet [19] model. Haris *et al.* [15] design a deep back-projection network for super-resolution by exploiting iterative up- and down- sampling layers. DSRN [14] introduces dual-state design that improved on memory consumption. The MSRN [28] and RFA [32] models use different blocks to efficiently exploit the image features. Recently, attention mechanisms are also widely used to improve the super-resolution image quality [66, 67, 5, 39, 41].

Numerous methods based on generative adversarial networks (GANs) have been developed to improve SISR quality, including SRGAN [27], EnhanceNet [43], ESRGAN [54], SPSR [38] and SRFlow [36]. These methods typically generate visual pleasing results by using GAN [12] losses or normalizing flows [42]. In addition, several methods have been developed to study more realistic degradation setup (e.g., downsampling kernels) for SISR [58, 13, 20, 64, 56].

### 2.2. Video super-resolution

Video super-resolution is considered to be a more challenging problem as both content and motion need to be effectively predicted. The motion information provides additional cues in restoring high-resolution frames from more than one low-resolution image.

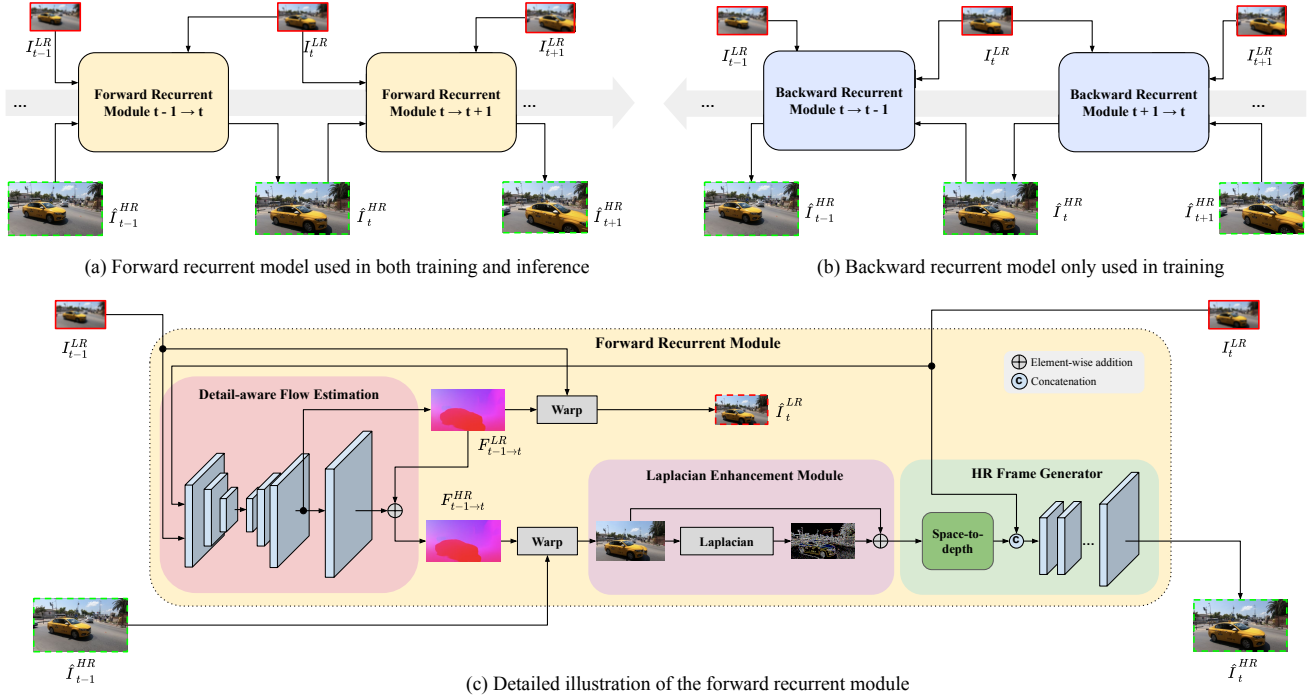


Figure 2. Overview of the COMISR model. The forward and backward recurrent module are symmetric and share the weights. In the figure, red rectangles represent the LR input frames and green dash-lined rectangles represent the HR predicted frames.

**Sliding-window methods.** Multi-frame super-resolution methods provide more robust solutions to restore high-resolution details of target frames from a number of input images (e.g., 5 to 7 frames). A number of models compute optical flows between multi-frames to aggregate information. Xue *et al.* [59] introduce a task-oriented flow estimation method together with a video processing network for denoising and super-resolution. Haris *et al.* [16] use multiple back-projected features for iterative refinement rather than explicitly aligning frames. Recently, deformable convolution networks [4] have been developed to tackle feature misalignment in dense prediction tasks. Both EDVR [52, 53] and TDAN [48] use deformable convolution to align features from video frames for video super-resolution. Haris *et al.* [17] design a space-time-aware network that leverages mutually informative relationships between time and space, and improves the performances on space-time, spatial and temporal VSR tasks. In [62], Yi *et al.* also explore the fusion of consecutive frames to fully exploit spatial-temporal information. Similarly, Li *et al.* [29] use inter and intra frame information to exploiting temporal and spatial correlation between frames.

**Recurrent methods.** Recurrent network structures are efficient and widely adapted in numerous vision tasks, such as classification [30, 7], detection [33, 50], and segmentation [51]. Such network models can process inputs of any length by sharing model weights across time. In addition,

recurrent models can take account for long-range dependence among pixels. A number of VSR models have been developed based on recurrent neural networks. The FRVSR [44] model stores the previous information in a HR frame for restoring the current frame in a sequence. Fuoli [11] use a recurrent latent space to encode and propagate temporal information among frames for video super-resolution. Most recently, the RSDN model [21], incorporates a structure-preserving module into a recurrent network, and achieves state-of-the-art performance for restoring details from LR frames without relying on motion compensation.

### 3. Proposed Method

The COMISR model is designed using the recurrent formulation. It feeds the previous information to the current frame, which is similar to the state-of-the-art video SR methods [44, 21]. The recurrent design usually entails low memory consumption, and can be applied to numerous inference tasks in videos.

Figure 2 shows an overview of the COMISR model. We design three novel modules, namely bi-directional recurrent warping, detail-aware flow estimation and Laplacian enhancement modules, to make the model robust to compressed videos. Given the LR ground truth frames, we apply forward and backward recurrent modules to generate the HR frame predictions, and compute content losses against

HR ground truth frames in both directions. In the recurrent module, we predict flows and generate warped frames in both LR and HR, and train the network end to end using the LR and HR ground truth frames.

### 3.1. Bi-directional Recurrent Module

One common technique used in video compression is to apply different algorithms to compress and encode frames at different positions in the video stream. Typically, a codec randomly selects several reference frames, known as the *intra-frames*, and compresses them independently without using information from other frames. It then compresses other frames by exploiting consistency and encoding differences from the *intra-frames*. As a result, the *intra-frames* usually require more bits to encode and have less compression artifacts than other frames. In video super-resolution, since the location of *intra-frames* is not known in advance, to effectively reduce the accumulated error from the unknown location of *intra-frames*, we propose a bi-directional recurrent network to enforce the forward and backward consistency of the LR warped inputs and HR predicted frames.

Specifically, the bi-directional recurrent network consists of symmetric modules for forward and backward directions. In the forward direction, we first estimate both the LR flow  $F_{t-1 \rightarrow t}^{LR}$  and HR one  $F_{t-1 \rightarrow t}^{HR}$  using the LR frames  $I_{t-1}^{LR}$  and  $I_t^{LR}$  (described in more detail in Section 3.2). We then apply different operations separately in LR and HR streams. In the LR stream, we warp the previous LR frame  $I_{t-1}^{LR}$  to time  $t$  using  $F_{t-1 \rightarrow t}^{LR}$  to obtain the warped LR frame  $\tilde{I}_t^{LR}$ , which will be used at later stages:

$$\tilde{I}_t^{LR} = \text{Warp}(I_{t-1}^{LR}, F_{t-1 \rightarrow t}^{LR}) \quad (1)$$

In the HR stream, we warp the previous predicted frames  $\hat{I}_{t-1}^{HR}$  to time  $t$  using  $F_{t-1 \rightarrow t}^{HR}$  to obtain the warped HR frame  $\hat{I}_t^{HR}$ , followed by a Laplacian Enhancement Module to generate accurate HR warped frame:

$$\hat{I}_t^{HR, \text{Warp}} = \text{Warp}(\hat{I}_{t-1}^{HR}, F_{t-1 \rightarrow t}^{HR}) \quad (2)$$

$$\tilde{I}_t^{HR} = \text{Laplacian}(\hat{I}_t^{HR, \text{Warp}}) + \hat{I}_t^{HR, \text{Warp}} \quad (3)$$

We then apply a space-to-depth operation on  $\tilde{I}_t^{HR}$  to shrink back its resolution while expanding its channel, fuse it with the LR input  $I_t^{LR}$  and pass the concatenated frame to the HR frame generator to get our final HR prediction  $\hat{I}_t^{HR}$ . We compare  $\hat{I}_t^{HR}$  with the ground truth HR  $I_t^{HR}$  to measure the loss.

Similarly, we apply the symmetric operations in the backward direction to obtain the warped LR frame and the predicted HR frame. In this case, the detail-aware flow estimation module generates the backward flow from time  $t$  to  $t-1$ , and warping is done by applying the backward flow to the frame at time  $t$  to estimate the frame at time  $t-1$ .

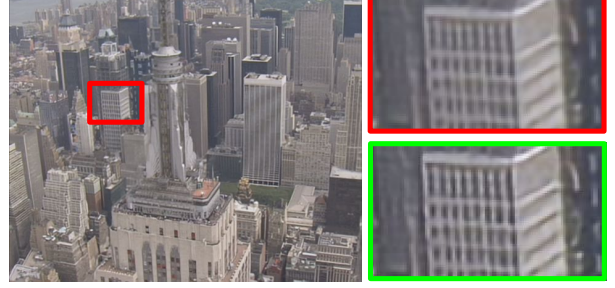


Figure 3. Laplacian image enhancement. The left image is an intermediate predicted HR frame in the training pipeline. The image patch in red box is from the intermediate predicted HR frame. The image patch in green box is with the Laplacian image added.

### 3.2. Detail-aware Flow Estimation

In our recurrent module, we explicitly estimate both the LR and HR flows between neighboring frames and pass this information in forward and backward directions.

Here we take the forward direction for illustration. The operations in the backward direction are similarly applied. We first concatenate two neighboring LR frames  $I_{t-1}^{LR}$  and  $I_t^{LR}$  and pass it through the LR flow estimation network to generate the LR flow  $F_{t-1 \rightarrow t}^{LR}$ . Instead of directly upsampling the LR flow  $F_{t-1 \rightarrow t}^{LR}$ , we add a few additional deconvolution layers on top of the bilinear upsampled LR flow. Thus, a detailed residual map is encouraged to be learnt during the end-to-end training, and consequently we can better preserve high-frequency details in the predicted HR flow.

### 3.3. Laplacian Enhancement Module

The Laplacian residual has been widely used in many vision tasks, including image blending, super-resolution, and restoration. It is particularly useful at finding the fine details from a video frame, where such details could be smoothed during video compression. In our recurrent VSR model, the warped predicted HR frame retains information and some details learned from the previous frames. Such details can be easily missing from the up-scaling network, as shown in Figure 2. As such, we add a Laplacian residual to a predicted HR frame to enhance details.

A Laplacian boosted image is computed by a Gaussian kernel blur  $G(\cdot, \cdot)$  with the width of  $\sigma$ :

$$\tilde{I}_t^{HR} = \hat{I}_t^{HR} + \alpha(\hat{I}_t^{HR} - G(\hat{I}_t^{HR}, \sigma = 1.5)) \quad (4)$$

where  $\hat{I}_t^{HR}$  is an intermediate results of the predicted HR frame and  $\alpha$  is weighted factor controls the residual power. Figure 3 shows a comparison of enhancing details using Laplacian images. Comparing image patch in red and green boxes, it is clear that the detailed texture has been sharpened. We present more ablation studies in Section 4 to demonstrate the effectiveness using the Laplacian residual for enhancing image details.



By exploiting the Laplacian, we add details back to the warped HR frame. This is followed by a space-to-depth operation, which rearranges blocks of spatial data into depth dimension, and then concatenation with the LR input frame. We pass it through the HR frame generator to generate the final HR prediction.

### 3.4. Loss Function

During training, there are two streams: the HR and LR frames. The losses are designed with consideration of using both of the streams. For loss on HR frames, the  $\mathcal{L}_2$  distance is computed between the final outputs and the HR frames. In Section 3.1, we described our bi-directional recurrent module for improving the model quality.  $I_t$  denotes the ground truth frame and  $\hat{I}_t$  denotes the generated frame at time  $t$ . For each of the recurrent steps, the predicted HR frames are used for computing loss. The  $\mathcal{L}_2$  losses are combined as,

$$\mathcal{L}_{content}^{HR} = \frac{1}{2N} \left( \underbrace{\sum_{t=1}^N \|I_t^{HR} - \hat{I}_t^{HR}\|_2}_{\text{forward}} + \underbrace{\sum_{t=N}^1 \|I_t^{HR} - \hat{I}_t^{HR}\|_2}_{\text{backward}} \right) \quad (5)$$

Each of the warped LR frames from  $t-1$  to  $t$  is penalized with the  $\mathcal{L}_2$  distance with respect to the current LR frame as,

$$\mathcal{L}_{warp}^{LR} = \frac{1}{2N} \left( \underbrace{\sum_{t=1}^N \|I_t^{LR} - \tilde{I}_{t-1}^{warp}\|_2}_{\text{forward}} + \underbrace{\sum_{t=N}^1 \|I_t^{LR} - \tilde{I}_{t-1}^{warp}\|_2}_{\text{backward}} \right) \quad (6)$$

The total loss is the sum of the HR and LR losses,

$$\mathcal{L}_{total} = \beta \mathcal{L}_{content}^{HR} + \gamma \mathcal{L}_{warp}^{LR} \quad (7)$$

where  $\beta$  and  $\gamma$  are weights for each loss.

## 4. Experiments

In this section, we first introduce our implementation details, including datasets, compression methods, training details, and evaluation metrics. We then compare our method with a few most recent state-of-the-art VSR models on common benchmark datasets. Both visual and quantitative results on a wide range of compression rates are presented. In addition, we demonstrate that our method is better than a separated denoiser followed by a VSR model. We also evaluate the COMISR model on real-world compressed YouTube videos. Finally, we show ablation study on the three novel modules with analysis. Note that more results and videos can be found in the supplementary material.

### 4.1. Implementation Details

**Datasets.** In our work, we use the REDS [40] and Vimeo [59] datasets for training. The REDS dataset contains more than 200 video sequences for training, each of

which has 100 frames with  $1280 \times 720$  resolution. The Vimeo-90K dataset contains about 65k video sequences for training, each of which has 7 frames with  $448 \times 256$  resolution. One main difference between these two datasets is the REDS dataset has much larger motion between consecutive frames captured from a hand-held device. To train and evaluate the COMISR model, the frames are first smoothed by a Gaussian kernel with width of 1.5 and downsampled by  $4\times$ .

We evaluate the COMISR model on the Vid4 [31] and REDS4 [40] datasets (clip# 000, 011, 015, 020). All the testing sequences have more than 30 frames. In the following experiments, the COMISR model evaluated on the REDS4 dataset is trained with the REDS dataset following the setting described in [52]. The COMISR model in all the other experiments is trained using the Vimeo-90K dataset.

**Compression Methods.** We follow the most common setting for the H.264 codec at different compression rates (i.e., different CRF values). The recommended CRF value is between 18 and 28, and the default is 23 (although the value ranges between 0 and 51). In our experiments, we use CRF of 15, 25, and 35 to evaluate video super-resolution with a wide range of compression rates. For fair comparisons, when evaluating other methods, we use the same degradation method to generate the LR sequences before compression. Finally, such compressed LR sequences are fed into the VSR models for inference.

**Training Process.** For each of the input frames, we randomly crop  $128 \times 128$  patches from a mini-batch as input. Each mini-batch consists of 16 samples. The  $\alpha$ ,  $\beta$ , and  $\gamma$  parameters described in Section 3 are set to 1, 20, 1, respectively. The model training is supervised by the losses described in the Section 3.4. We use the Adam optimizer [25] with  $\beta_1 = 0.9$  and  $\beta_2 = 0.999$ . The learning rate is set to  $5 \times 10^{-5}$ . We adopt video compression as an additional data augmentation method to the training pipeline with a probability of 50% on the input batches. Such augmentation is added during the last 20% of the training epochs. The FFmpeg codec is employed for the compression with a CRF value randomly selected between 15 and 25. All the models were trained on 8 NVidia Tesla V100 GPUs. The source code, datasets, and trained models will be made available to the public.

**Evaluation Metrics.** We use PSNR, SSIM, and LPIPS [65] for quantitative evaluation of video super-resolution results. For evaluations on YouTube videos, we only present visual examples for comparison since ground-truth frames are not available.

### 4.2. Evaluation against the State-of-the-Arts

We evaluate the COMISR model against state-of-the-art VSR methods, including FRVSR [44], DUF [22],



Figure 4. Qualitative evaluation on the Vid4 dataset for  $4\times$  VSR. Our model can recover more structure details such as faces and boundaries, with much fewer artifacts. Zoom in for best view.

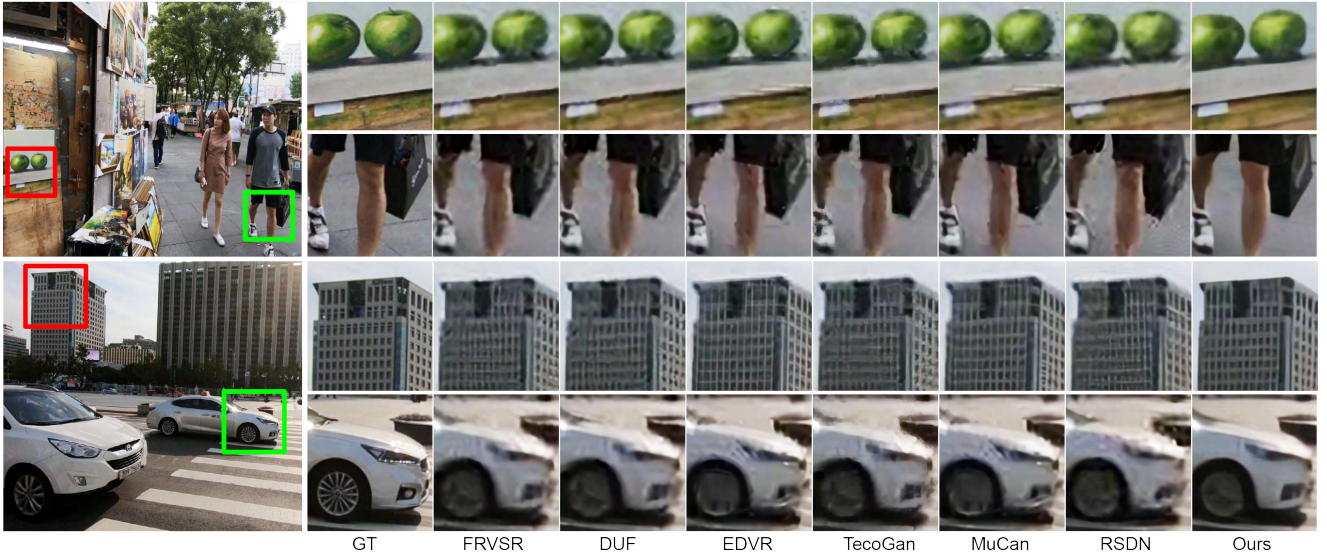


Figure 5. Qualitative results on videos from the REDS4 dataset  $4\times$  VSR. Our model achieves much better quality on detailed textures, with much fewer artifacts. The brightness of the pictures is increased by 60 for better viewing. Zoom in for best view.

EDVR [52], TecoGan [3], MuCAN [29], and RSDN [21]. Three of the evaluated methods are based on recurrent models, whereas the other three are using a temporal sliding window (between 5 and 7 frames). When available, we use the original code and trained models, and otherwise implement these methods. For fair comparison, the LR frames have been generated exactly as described in their published work. These LR frames are then compressed and fed into the super-resolution networks for evaluation.

For the Vid4 dataset [31], the quantitative metrics PSNR and SSIM are computed on both the Y-channel and RGB-channels, as shown in Table 1. We present the averaged performance on uncompressed videos (original sequence), and

with a range of compression factors (15, 25, 35). We also report the individual sequence performance under CRF25. More results on other CRF factors are presented in the supplementary material. Overall, the COMISR method outperforms all the compared methods on a mid-to-high compression rate by 0.5-1.0db on PSNR. Meanwhile, our method maintains competitive performance (2nd or 3rd place) in less compressed videos. Figure 4 shows some results by the evaluated methods from two sequences. The COMISR model can recover more details from the LR frames with fewer compression artifacts. Both quantitative and visual results show that the COMISR method achieves the state-of-the-art results on compressed videos.

Model	FLOPs #Param.	CRF 25					No compression -	Compressed Results			
		calendar	city	foliage	walk			CRF15	CRF25	CRF35	
FRVSR [44]	0.05T	21.55 / 0.631	25.40 / 0.575	24.11 / 0.625	26.21 / 0.764		26.71 / 0.820	26.01 / 0.766	24.33 / 0.655	22.05 / 0.482	
	2.53M	19.75 / 0.606	23.79 / 0.572	24.49 / 0.751	25.22 / 0.815		25.22 / 0.815	24.38 / 0.753	22.59 / 0.640	20.35 / 0.469	
DUF [22]	0.62T	21.16 / 0.634	23.78 / 0.632	22.97 / 0.603	24.33 / 0.771		27.33 / 0.832	24.40 / 0.773	23.06 / 0.660	21.27 / 0.515	
	5.82M	19.40 / 0.588	22.25 / 0.594	21.30 / 0.567	22.66 / 0.737		25.79 / 0.814	22.81 / 0.744	21.41 / 0.621	19.61 / 0.468	
EDVR [52]	0.93T	21.69 / 0.648	25.51 / 0.626	24.01 / 0.606	26.72 / 0.786		27.35 / 0.826	26.34 / 0.771	24.45 / 0.667	22.31 / 0.534	
	20.6M	19.87 / 0.599	23.90 / 0.586	22.27 / 0.570	24.89 / 0.754		25.85 / 0.808	24.67 / 0.740	22.73 / 0.627	20.62 / 0.487	
TecoGan [3]	0.14T	21.34 / 0.624	25.26 / 0.561	23.50 / 0.592	25.73 / 0.756		25.88 / 0.794	25.25 / 0.741	23.94 / 0.639	21.99 / 0.479	
	5.05M	19.55 / 0.601	23.65 / 0.559	21.73 / 0.573	24.40 / 0.743		24.34 / 0.788	23.61 / 0.728	22.22 / 0.624	20.28 / 0.466	
MuCAN [29]	-	21.60 / 0.643	25.38 / 0.620	23.93 / 0.599	26.43 / 0.782		27.26 / 0.822	25.85 / 0.753	24.34 / 0.661	22.26 / 0.531	
	-	19.81 / 0.597	23.78 / 0.581	22.20 / 0.564	24.72 / 0.750		25.56 / 0.801	24.22 / 0.725	22.63 / 0.623	20.57 / 0.485	
RSDN [21]	0.13T	21.72 / 0.650	25.28 / 0.615	23.69 / 0.591	25.57 / 0.747		<b>27.92 / 0.851</b>	<b>26.58 / 0.781</b>	24.06 / 0.650	21.29 / 0.483	
	6.19M	19.89 / 0.599	23.68 / 0.575	21.94 / 0.554	23.91 / 0.711		26.43 / 0.835	24.88 / 0.750	22.36 / 0.610	19.67 / 0.437	
Ours	0.06T	<b>22.81 / 0.695</b>	<b>25.94 / 0.640</b>	<b>24.66 / 0.656</b>	<b>26.95 / 0.799</b>		27.31 / 0.840	26.43 / 0.791	<b>24.97 / 0.701</b>	<b>22.35 / 0.509</b>	
	2.63M	20.39 / 0.667	24.30 / 0.633	22.88 / 0.638	25.21 / 0.788		25.79 / 0.835	24.76 / 0.778	23.21 / 0.686	20.66 / 0.494	

Table 1. Performance evaluation on compressed Vid4 videos. For each entry, the first row is PSNR/SSIM on Y channel, and the second row is PSNR/SSIM on RGB channels. The best method on the Y channel for each column is highlighted in bold and shade. The FLOPs are reported based on the Vid4 4× VSR. The FLOPs and #Param of FRVSR is based on our implementation.

Model	#Frame	CRF 25				No compression -	Compressed Results			
		clip_000	clip_011	clip_015	clip_020		CRF15	CRF25	CRF35	
FRVSR [44]	recur(2)	24.25 / 0.631	25.65 / 0.687	28.17 / 0.770	24.79 / 0.694		28.55 / 0.838	27.61 / 0.784	25.72 / 0.696	23.22 / 0.579
DUF [22]	7	23.46 / 0.622	24.02 / 0.686	25.76 / 0.773	23.54 / 0.689		28.63 / 0.825	25.61 / 0.775	24.19 / 0.692	22.17 / 0.588
EDVR [52]	7	24.38 / 0.629	26.01 / 0.702	28.30 / 0.783	25.21 / 0.708		<b>31.08 / 0.880</b>	<b>28.72 / 0.805</b>	25.98 / 0.706	23.36 / 0.600
TecoGan [3]	recur(2)	24.01 / 0.624	25.39 / 0.682	27.95 / 0.768	24.48 / 0.686		27.63 / 0.815	26.93 / 0.768	25.46 / 0.690	22.95 / 0.589
MuCAN [29]	5	24.39 / 0.628	26.02 / 0.702	28.25 / 0.781	25.17 / 0.707		30.88 / 0.875	28.67 / 0.804	25.96 / 0.705	23.55 / 0.600
RSDN [21]	recur(2)	24.04 / 0.602	25.40 / 0.673	27.93 / 0.766	24.54 / 0.676		29.11 / 0.837	27.66 / 0.768	25.48 / 0.679	23.03 / 0.579
Ours	recur(2)	<b>24.76 / 0.660</b>	<b>26.54 / 0.722</b>	<b>29.14 / 0.805</b>	<b>25.44 / 0.724</b>		29.68 / 0.868	28.40 / 0.809	<b>26.47 / 0.728</b>	<b>23.56 / 0.599</b>

Table 2. Performance evaluation on compressed the REDS4 dataset. Each entry shows the PSNR/SSIM on RGB channels. The best method for each column is highlighted in bold and shade, and recur(2) indicates a recurrent network using 2 frames.

We also evaluate the COMISR model against the state-of-the-art methods on the REDS4 dataset [40]. Unlike the Vid4 dataset, the sequences in this set are longer (100 frames) and more challenging with larger motion between frames. Table 2 shows the COMISR model achieves the best performance on the compressed videos from the REDS4 dataset. Figure 5 shows that our method is able to recover more details such as texture from the bricks on the sidewalk and windows on buildings.

There is an inherent trade-off between low-level structure accuracy (e.g., PSNR or SSIM) and high-level perceptual quality [2]. Perceptual distortion cannot be well characterized by such low-level structure accuracy. In this work, we use the LPIPS [65] metric for performance evaluation. Table 3 show the evaluation results using the LPIPS metric on both Vid4 and REDS4 datasets. Overall, the COMISR model performs well against the state-of-the-art methods on both datasets using the LPIPS metric (either second best on the Vid4 dataset or best on the more challenging REDS4 dataset).

We show video super-resolution results in the supplementary material. Although the compression artifacts are not easily observable in the LR frames, such artifacts are amplified and easily seen after super-resolution. For the compressed videos, the COMISR model effectively recovers more details from the input videos with fewer artifacts.

	FRVSR	TecoGan	DUF	EDVR	MuCAN	RSDN	OURS
Vid4	4.105	<b>3.245</b>	4.010	4.396	3.985	4.292	3.689
REDS4	4.188	3.643	4.223	4.075	4.085	4.423	<b>3.384</b>

Table 3. Performance evaluation using the LPIPS [65] metric (lower is better). Our method performs well, especially on the and more challenging REDS4 dataset.

### 4.3. VSR Schemes on Denoised Videos

As shown in Figure 4 and Figure 5, the COMISR model generates high-quality frames with fewer artifacts from compressed videos. An interesting question is that whether the state-of-the-art methods can achieve better results if the compressed videos are first denoised. As such, we use the state-of-the-art compressed video quality enhancement, STDF [6], for evaluation.

Using the settings described in Section 4.2, we compress video frames using CRF25. The STDF is then used to remove the video compression artifacts and generate enhanced LR frames as inputs for the state-of-the-art VSR methods. Table 4 shows the quantitative results by the COMISR model and the state-of-the-art VSR methods on videos denoised by the STDF scheme. We note that the performance of all of the compared method drops on the denoised LR frames. This can be attributed to that a separated denoising step is not compatible with the learned degradation kernel from the VSR methods. In addition, as reported





Figure 6. 4 $\times$  VSR results on REDS4 videos downloaded from YouTube with resolution of 360 pixels. Zoom in for best view

Model	VSR only		Video Denoiser + VSR	
	Y-Channel	RGB-Channels	Y-Channel	RGB-Channels
EDVR	24.45 / 0.667	22.73 / 0.627	22.56 / 0.581	20.94 / 0.541
TecoGan	23.94 / 0.639	22.22 / 0.624	22.25 / 0.541	20.63 / 0.530
MuCan	24.34 / 0.661	22.63 / 0.623	22.47 / 0.577	20.87 / 0.538
RSDN	24.06 / 0.650	22.36 / 0.610	22.19 / 0.560	20.59 / 0.520
OURS	<b>24.97 / 0.701</b>	<b>23.21 / 0.686</b>	-	-

Table 4. Ablation study on applying a video denoiser to the compressed frames before the VSR models using the Vid4 dataset. Each entry shows the PSNR/SSIM results on the Y or RGB channel. The COMISR model outperforms the state-of-the-art VSR methods with the STDF [6] denoiser.

in Section 4.5, simply adding compression augmentation to the existing model training would not perform well. These results show that the COMISR model is able to efficiently recover more details from compressed videos, and outperforms state-of-the-art models on denoised videos.

#### 4.4. Evaluation on Real-World Compressed Videos

Most videos on the web are compressed where frames can be preprocessed by a combination of unknown methods. We use the videos from the REDS4 testing dataset (see Section 4.2) for experiments as the image resolution is higher.

We first generate uncompressed videos out of the raw frames, and then upload them to YouTube. YouTube will transcode them and produce a few downsampled resolutions available for downloading. In our setting, the uploaded videos are 1280 $\times$ 720. The resolutions that are available for downloading on YouTube are 480, 360, 240, and 144 pixels. In the following experiments, we download the videos of 360 pixels using the YouTube-dl [63]. We evaluate three state-of-the-art methods, including MuCAN [29], RSDN [21], and TecoGan [3] on these videos that are compressed by unknown methods by Youtube. Figure 6 shows the VSR results by the evaluated methods. More videos and user study results are presented in the supplementary material.

#### 4.5. Ablation Study

We analyze the contribution of each module in the COMISR model. We start with the basic recurrent mod-

Components	No compression Aug		Aug CRF15-25	
	Uncompressed	CRF25	Uncompressed	CRF25
Recur	26.61 / 0.808	23.97 / 0.634	26.53 / 0.815	24.23 / 0.648
Recur + a	27.16 / 0.837	24.24 / 0.650	26.64 / 0.818	24.74 / 0.686
Recur + ab	27.45 / 0.844	24.27 / 0.649	27.27 / 0.838	24.92 / 0.696
Recur + abc	27.48 / 0.845	24.31 / 0.650	27.31 / 0.840	24.97 / 0.701

Table 5. Ablations on three modules of the COMISR model on Vid4: (a) bi-directional recurrent module, (b) detail-aware flow estimation, and (c) Laplacian enhancement module. Each entry shows the PSNR/SSIM values on the Y-channel.

ule described in Section 3 as the baseline model. Similar to FRVSR [44], the basic recurrent model computes the flow between consecutive frames, warps the previous frame to the current, and upscales the frames. We carry out two sets of ablation studies to show the effectiveness of each module: one without compression augmentation and the other with compression augmentation (see Section 4.1).

Table 5 shows the ablation studies where we incrementally add each module to the basic recurrent model. For each setting, the model is trained with and without compression augmentation, and then evaluated on original and compressed frames. The results show that each module helps achieve additional performance gain, in both training process with or without compression augmentation. In addition, compression augmentation plays an important role in achieving additional performance gain on compressed videos. The full COMISR model performs best among all settings. The compression augmentation slightly affects the performance on the original input videos. For example, the fourth row in Table 5, the uncompressed PSNR on Vid4 drops 0.17 dB.

## 5. Conclusion

In this work, we presented a compression-informed video super-resolution model which is robust and effective on compressed videos. Within an efficient recurrent network framework, we designed three modules to effectively recover more details from the compressed frames. We conducted extensive experiments on challenging video with a wide range of compression factors. The proposed COMISR model achieved the state-of-the-art performance on compressed videos qualitatively and quantitatively, while performing well on uncompressed videos.



## References

- [1] Saeed Anwar, Salman Khan, and Nick Barnes. A deep journey into super-resolution: A survey. *ACM Computing Surveys*, 2020. 2
- [2] Y. Blau and T. Michaeli. The perception-distortion tradeoff. In *CVPR*, 2018. 7
- [3] Mengyu Chu, You Xie, Jonas Mayer, Laura Leal-Taixe, and Nils Thuerey. Learning temporal coherence via self-supervision for gan-based video generation. *ACM Transactions on Graphics*, 2018. 6, 7, 8, 11, 12
- [4] Jifeng Dai, Haozhi Qi, Yuwen Xiong, Yi Li, Guodong Zhang, Han Hu, and Yichen Wei. Deformable convolutional networks. In *ICCV*, 2017. 3
- [5] Tao Dai, Jianrui Cai, Yongbing Zhang, Shu-Tao Xia, and Lei Zhang. Second-order attention network for single image super-resolution. In *CVPR*, 2019. 2
- [6] Jianing Deng, Li Wang, Shiliang Pu, and Cheng Zhuo. Spatio-temporal deformable convolution for compressed video quality enhancement. In *AAAI*, 2020. 7, 8
- [7] J. Donahue, L. A. Hendricks, M. Rohrbach, S. Venugopalan, S. Guadarrama, K. Saenko, and T. Darrell. Long-term recurrent convolutional networks for visual recognition and description. *IEEE Transactions on Pattern Analysis and Machine Intelligence*, 39(4):677–691, 2017. 3
- [8] Chao Dong, Chen Change Loy, Kaiming He, and Xiaoou Tang. Learning a deep convolutional network for image super-resolution. In *ECCV*, 2014. 2
- [9] Chao Dong, Chen Change Loy, and Xiaoou Tang. Accelerating the super-resolution convolutional neural network. In *ECCV*, 2016. 2
- [10] FFmpeg. FFmpeg h.264 video encoding guide. In <https://trac.ffmpeg.org/wiki/Encode/H.264>. 1
- [11] Dario Fuoli, Shuhang Gu, and Radu Timofte. Efficient video super-resolution through recurrent latent space propagation. In *ICCV Workshops*, 2019. 3
- [12] Ian J. Goodfellow, Jean Pouget-Abadie, Mehdi Mirza, Bing Xu, David Warde-Farley, Sherjil Ozair, Aaron Courville, and Yoshua Bengio. Generative adversarial nets. In *NeurIPS*, 2014. 2
- [13] Yong Guo, Jian Chen, Jingdong Wang, Qi Chen, Jiezhong Cao, Zeshuai Deng, Yanwu Xu, and Minghui Tan. Closed-loop matters: Dual regression networks for single image super-resolution. In *CVPR*, 2020. 2
- [14] Wei Han, Shiyu Chang, Ding Liu, Mo Yu, Michael Witbrock, and Thomas S. Huang. Image super-resolution via dual-state recurrent networks. In *CVPR*, 2018. 2
- [15] Muhammad Haris, Gregory Shakhnarovich, and Norimichi Ukita. Deep back-projection networks for super-resolution. In *CVPR*, 2018. 2
- [16] Muhammad Haris, Greg Shakhnarovich, and Norimichi Ukita. Recurrent back-projection network for video super-resolution. In *CVPR*, 2019. 3
- [17] Muhammad Haris, Greg Shakhnarovich, and Norimichi Ukita. Space-time-aware multi-resolution video enhancement. In *CVPR*, 2020. 3
- [18] Kaiming He, Xiangyu Zhang, Shaoqing Ren, and Jian Sun. Deep residual learning for image recognition. *arXiv preprint arXiv:1512.03385*, 2015. 2
- [19] Gao Huang, Zhuang Liu, Laurens van der Maaten, and Kilian Q. Weinberger. Densely connected convolutional networks. In *CVPR*, 2017. 2
- [20] Shady Abu Hussein, Tom Tirer, and Raja Giryes. Correction filter for single image super-resolution: Robustifying off-the-shelf deep super-resolvers. In *CVPR*, 2020. 2
- [21] Takashi Isobe, Xu Jia, Shuhang Gu, Songjiang Li, Shengjin Wang, and Qi Tian. Video super-resolution with recurrent structure-detail network. In *ECCV*, 2020. 3, 6, 7, 8, 11, 12
- [22] Younghyun Jo, Seoung Wug Oh, Jaeyeon Kang, and Seon Joo Kim. Deep video super-resolution network using dynamic upsampling filters without explicit motion compensation. In *CVPR*, 2018. 5, 7
- [23] Jiwon Kim, Jung Kwon Lee, and Kyoung Mu Lee. Accurate image super-resolution using very deep convolutional networks. In *CVPR*, 2016. 2
- [24] Jiwon Kim, Jung Kwon Lee, and Kyoung Mu Lee. Deeply-recursive convolutional network for image super-resolution. In *CVPR*, 2016. 2
- [25] Diederik P. Kingma and Jimmy Ba. Adam: A method for stochastic optimization. In *ICLR*, 2015. 5
- [26] Wei-Sheng Lai, Jia-Bin Huang, Narendra Ahuja, and Ming-Hsuan Yang. Deep laplacian pyramid networks for fast and accurate super-resolution. In *CVPR*, 2017. 2
- [27] Christian Ledig, Lucas Theis, Ferenc Huszar, Jose Caballero, Andrew Cunningham, Alejandro Acosta, Andrew Aitken, Alykhan Tejani, Johannes Totz, Zehan Wang, and Wenzhe Shi. Photo-realistic single image super-resolution using a generative adversarial network. In *CVPR*, 2017. 2
- [28] Juncheng Li, Faming Fang, Kangfu Mei, and Guixu Zhang. Multi-scale residual network for image super-resolution. In *ECCV*, 2018. 2
- [29] Wenbo Li, Xin Tao, Taian Guo, Lu Qi, Jiangbo Lu, and Jiaya Jia. Mucan: Multi-correspondence aggregation network for video super-resolution. In *ECCV*, 2020. 3, 6, 7, 8
- [30] Ming Liang and Xiaolin Hu. Recurrent convolutional neural network for object recognition. In *CVPR*, June 2015. 3
- [31] C. Liu and D. Sun. A Bayesian approach to adaptive video super resolution. In *CVPR*, 2011. 1, 2, 5, 6, 11
- [32] Jie Liu, Wenjie Zhang, Yuting Tang, Jie Tang, and Gangshan Wu. Residual feature aggregation network for image super-resolution. In *CVPR*, 2020. 2
- [33] Mason Liu, Menglong Zhu, Marie White, Yinxiao Li, and Dmitry Kalenichenko. Looking fast and slow: Memory-guided mobile video object detection, 2019. 3
- [34] Guo Lu, Wanli Ouyang, Dong Xu, Xiaoyun Zhang, Zhiyong Gao, and Ming-Ting Sun. Deep kalman filtering network for video compression artifact reduction. In *ECCV*, 2018. 1
- [35] G. Lu, X. Zhang, W. Ouyang, D. Xu, L. Chen, and Z. Gao. Deep non-local kalman network for video compression artifact reduction. *IEEE Transactions on Image Processing*, 29:1725–1737, 2020. 1
- [36] Andreas Lugmayr, Martin Danelljan, Luc Van Gool, and Radu Timofte. Srfnet: Learning the super-resolution space with normalizing flow. In *ECCV*, 2020. 2

- [37] Xiaotong Luo, Yuan Xie, Yulun Zhang, Yanyun Qu, Cuihua Li, and Yun Fu. Latticenet: Towards lightweight image super-resolution with lattice block. In *ECCV*, 2020. 2
- [38] Cheng Ma, Yongming Rao, Yean Cheng, Ce Chen, Jiwen Lu, and Jie Zhou. Structure-preserving super resolution with gradient guidance. In *CVPR*, 2020. 2
- [39] Yiqun Mei, Yuchen Fan, Yuqian Zhou, Lichao Huang, Thomas S. Huang, and Honghui Shi. Image super-resolution with cross-scale non-local attention and exhaustive self-exemplars mining. In *CVPR*, 2020. 2
- [40] Seungjun Nah, Sungyong Baik, Seokil Hong, Gyeongsik Moon, Sanghyun Son, Radu Timofte, and Kyoung Mu Lee. Ntire 2019 challenge on video deblurring and super-resolution: Dataset and study. In *CVPR Workshops*, 2019. 2, 5, 7, 11
- [41] Ben Niu, Weilei Wen, Wenqi Ren, Xiangde Zhang, Lianping Yang, Shuzhen Wang, Kaihao Zhang, Xiaochun Cao, and Haifeng Shen. Single image super-resolution via a holistic attention network. In *ECCV*, 2020. 2
- [42] Danilo Rezende and Shakir Mohamed. Variational inference with normalizing flows. In *ICML*, 2015. 2
- [43] Mehdi S. M. Sajjadi, Bernhard Scholkopf, and Michael Hirsch. Enhancenet: Single image super-resolution through automated texture synthesis. In *ICCV*, 2017. 2
- [44] Mehdi S. M. Sajjadi, Raviteja Vemulapalli, and Matthew Brown. Frame-Recurrent Video Super-Resolution. In *CVPR*, 2018. 3, 5, 7, 8, 11, 12
- [45] M. Schuster and K. K. Paliwal. Bidirectional recurrent neural networks. *IEEE Transactions on Signal Processing*, 45(11):2673–2681, 1997. 2
- [46] Wenzhe Shi, Jose Caballero, Ferenc Huszar, Johannes Totz, Andrew P. Aitken, Rob Bishop, Daniel Rueckert, and Zehan Wang. Real-time single image and video super-resolution using an efficient sub-pixel convolutional neural network. In *CVPR*, 2016. 2
- [47] Ying Tai, Jian Yang, Xiaoming Liu, and Chunyan Xu. Memnet: A persistent memory network for image restoration. In *ICCV*, 2017. 2
- [48] Yapeng Tian, Yulun Zhang, Yun Fu, and Chenliang Xu. Tdan: Temporally-deformable alignment network for video super-resolution. In *CVPR*, 2020. 3
- [49] Tong Tong, Gen Li, Xiejie Liu, and Qinquan Gao. Image super-resolution using dense skip connections. In *ICCV*, 2017. 2
- [50] Vivek Veeriah, Naifan Zhuang, and Guo-Jun Qi. Differential recurrent neural networks for action recognition. In *ICCV*, December 2015. 3
- [51] Carles Ventura, Miriam Bellver, Andreu Girbau, Amaia Salvador, Ferran Marques, and Xavier Giro-i Nieto. Rvos: End-to-end recurrent network for video object segmentation. In *CVPR*, June 2019. 3
- [52] Xintao Wang, Kelvin C.K. Chan, Ke Yu, Chao Dong, and Chen Change Loy. Edvr: Video restoration with enhanced deformable convolutional networks. In *CVPR Workshops*, 2019. 3, 5, 6, 7, 11, 12
- [53] Xintao Wang, Ke Yu, Kelvin C.K. Chan, Chao Dong, and Chen Change Loy. Basicsr. <https://github.com/xinntao/BasicSR>, 2020. 3
- [54] Xintao Wang, Ke Yu, Shixiang Wu, Jinjin Gu, Yihao Liu, Chao Dong, Yu Qiao, and Chen Change Loy. Esrgan: Enhanced super-resolution generative adversarial networks. In *ECCV Workshops*, 2018. 2
- [55] Z. Wang, J. Chen, and S. C. H. Hoi. Deep learning for image super-resolution: A survey. *IEEE Transactions on Pattern Analysis and Machine Intelligence*, 2020. 1, 2
- [56] Pengxu Wei, Ziwei Xie, Hannan Lu, Zongyuan Zhan, Qixiang Ye, Wangmeng Zuo, and Liang Lin. Component divide-and-conquer for real-world image super-resolution. In *ECCV*, 2020. 2
- [57] Yi Xu, Longwen Gao, Kai Tian, Shuigeng Zhou, and Huyang Sun. Non-local convlstm for video compression artifact reduction. In *ICCV*, 2019. 1
- [58] Yu-Syuan Xu, Shou-Yao Roy Tseng, Yu Tseng, Hsien-Kai Kuo, and Yi-Min Tsai. Unified dynamic convolutional network for super-resolution with variational degradations. In *CVPR*, 2020. 2
- [59] Tianfan Xue, Baian Chen, Jiajun Wu, Donglai Wei, and William T Freeman. Video enhancement with task-oriented flow. *International Journal of Computer Vision*, 2019. 3, 5, 11
- [60] Chih-Yuan Yang, Chao Ma, and Ming-Hsuan Yang. Single-image super-resolution: A benchmark. In *ECCV*, pages 372–386, 2014. 2
- [61] W. Yang, X. Zhang, Y. Tian, W. Wang, J. Xue, and Q. Liao. Deep learning for single image super-resolution: A brief review. *IEEE Transactions on Multimedia*, 2019. 2
- [62] Peng Yi, Zhongyuan Wang, Kui Jiang, Junjun Jiang, and Jiayi Ma. Progressive fusion video super-resolution network via exploiting non-local spatio-temporal correlations. In *ICCV*, 2019. 3
- [63] Youtube-dl. Youtube-downloader. In <https://github.com/yt-dl-org/youtube-dl>, 2021. 8
- [64] Kai Zhang, Luc Van Gool, and Radu Timofte. Deep unfolding network for image super-resolution. In *CVPR*, 2020. 2
- [65] Richard Zhang, Phillip Isola, Alexei A Efros, Eli Shechtman, and Oliver Wang. The unreasonable effectiveness of deep features as a perceptual metric. In *CVPR*, 2018. 5, 7
- [66] Yulun Zhang, Kunpeng Li, Kai Li, Lichen Wang, Bineng Zhong, and Yun Fu. Image super-resolution using very deep residual channel attention networks. In *ECCV*, 2018. 2
- [67] Yulun Zhang, Kunpeng Li, Kai Li, Bineng Zhong, and Yun Fu. Residual non-local attention networks for image restoration. In *ICLR*, 2019. 2
- [68] Yulun Zhang, Yapeng Tian, Yu Kong, Bineng Zhong, and Yun Fu. Residual dense network for image super-resolution. In *CVPR*, 2018. 2



Vid4 User Study

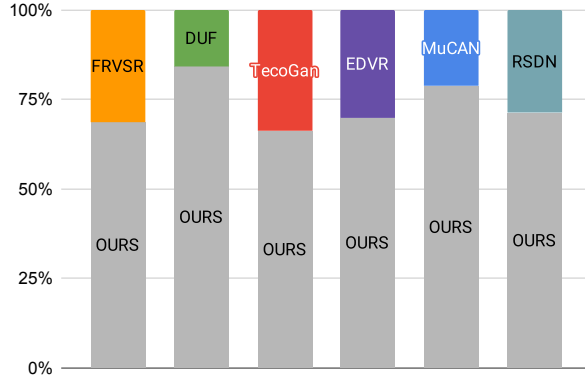


Figure 9. Vid4 user study results. All four sequences are used. The comparison is between COMISR and all other methods. Results show that users favored COMISR against all other compared methods.

REDS4 User Study

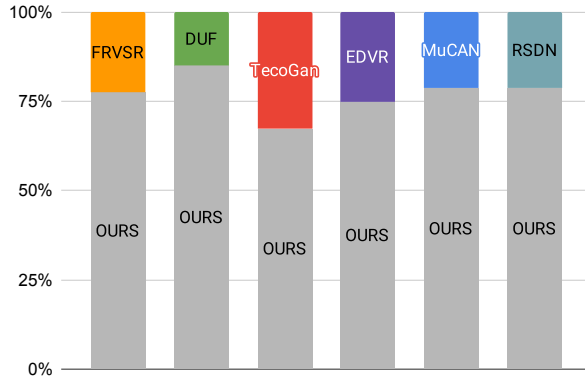


Figure 10. REDS4 user study results. All four sequences are used. The comparison is between COMISR and all other methods. Results show that users favored COMISR against all other compared methods.

Vimeo90K-T User Study

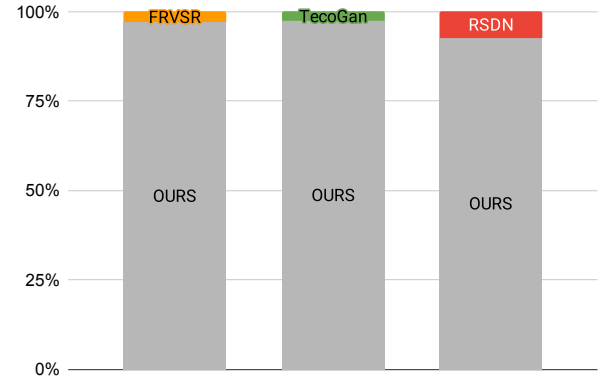


Figure 11. Vimeo90k testing set user study results. The first 20 sequences are used. The comparison is between COMISR and three other methods. Results show that users greatly favored COMISR against all other compared methods.

	Uncompressed	CRF25
FRVSR [44]	35.64 / 0.932	30.07 / 0.788
TecoGan [3]	34.07 / 0.909	29.84 / 0.784
EDVR [52]	37.61 / 0.949	30.53 / 0.844
RSDN [21]	37.23 / 0.947	29.63 / 0.815
OURS	35.71 / 0.926	31.05 / 0.816

Table 6. Performance evaluation of Y-channel on the Vimeo90K testing set.





Figure 12. Visual example of the Vid4 dataset. All the LR input frames are compressed with CRF25. Zoom in for best view.

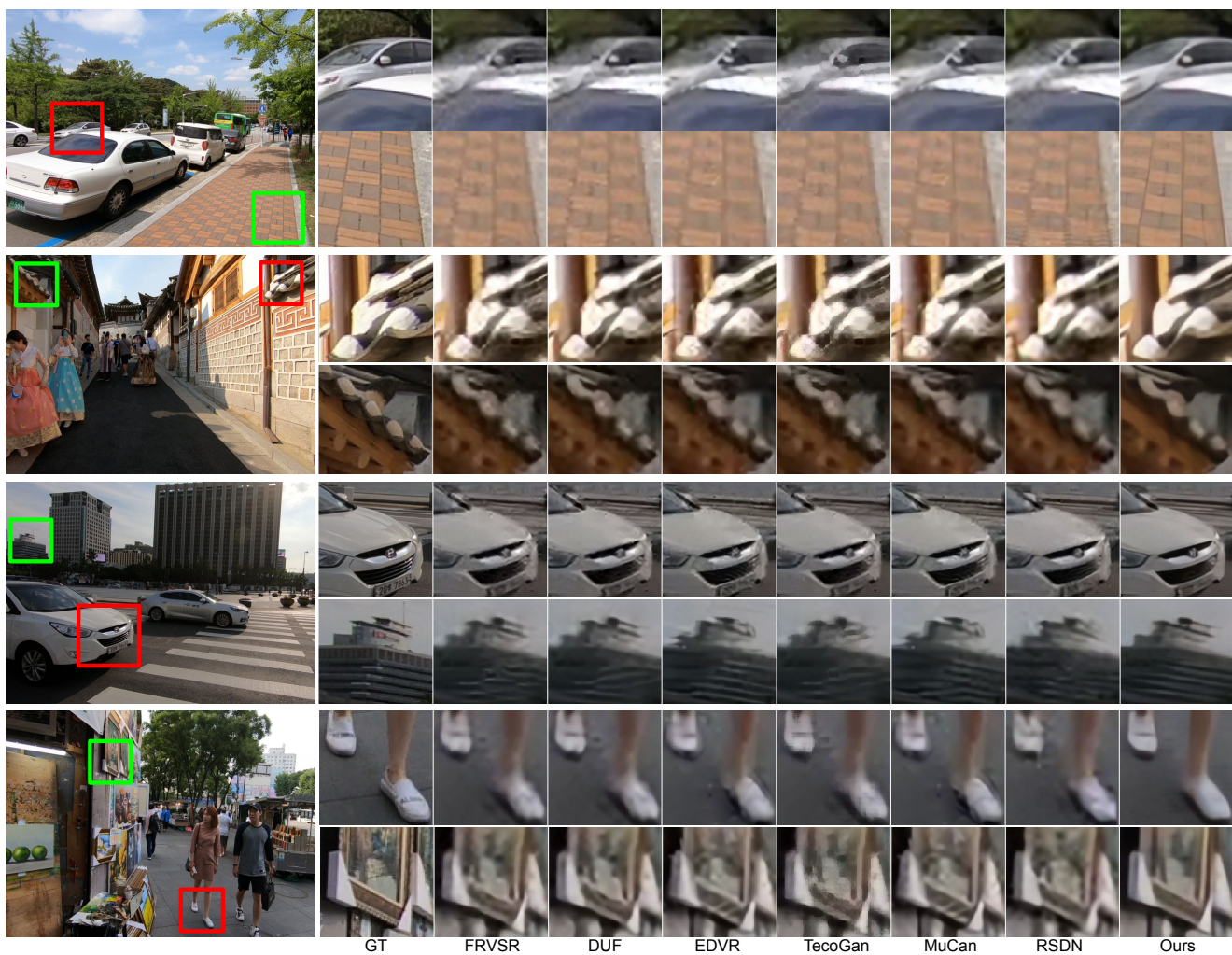


Figure 13. Visual example of the REDS4 dataset. All the LR input frames are compressed with CRF25. Zoom in for best view.